RSC Advances

PAPER

View Article Online
View Journal | View Issue

Cite this: *RSC Adv.*, 2023, **13**, 19955

Degradation mechanisms of organic compounds in molten hydroxide salts: a radical reaction yielding H_2 and graphite†

Florent Lecomte,[ac] Ana Gabriela Porras Guiterrez,[c] Marielle Huvé,[a] Alain Moissette,[b] Giuseppe Sicoli,[b] Anne-Laure Rollet*[c] and Sylvie Daviero-Minaud*[a]

Received 17th April 2023
Accepted 7th June 2023

DOI: 10.1039/d3ra02537c

rsc.li/rsc-advances

Molten salts are used in various waste treatments, such as recycling, recovery or making inert. Here, we present a study of the degradation mechanisms of organic compounds in molten hydroxide salts. Molten salt oxidation (MSO) using carbonates, hydroxides and chlorides is known for the treatment of hazardous waste, organic material or metal recovery. This process is described as an oxidation reaction due to the consumption of O_2 and formation of H_2O and CO_2. We have treated various organic products, carboxylic acids, polyethylene and neoprene with molten hydroxides at 400 °C. However, the reaction products obtained in these salts, especially carbon graphite and H_2 without CO_2 emission, challenges the previous mechanisms described for the MSO process. Combining several analyses of the solid residues and the gas produced during the reaction of organic compounds in molten hydroxides (NaOH–KOH), we demonstrate that these mechanisms are radical-based instead of oxidative. We also show that the obtained end products are highly recoverable graphite and H_2, which opens a new way of recycling plastic residues.

1 Introduction

Nowadays, the treatment of organic waste in Europe mainly relies on four different processes: incineration, recycling, methanisation and composting. Unfortunately, none of these processes can treat the whole variety of organic waste. Concerning plastics,[1] 32.5% are recycled, 24.9% are directly landfilled or used for energy recovery (methanisation for biodegradable plastics), and 42.6% are incinerated. Furthermore, waste formed by a mixture of materials (cardboard, metals, plastics, glass, *etc.*) are particularly challenging to process, and obviously cannot be composted or methanised.

Therefore, new treatments have to be developed to treat and valorise these wastes. In recent years, the Molten Salt Oxidation process (MSO) using molten carbonates has been put forward for the gasification of organic wastes[2] and even chlorinated organics.[3,4] This pyrochemical process allows the treatment of wastes at lower temperatures than incineration, with the absorption of acid gases,[5] absence of carbon monoxide gas emission[6] and degradation of fumes without any formation of dioxins.[7] Furthermore, the MSO process results in the decomposition of organic materials by oxidation until CO_2 is released at the end of the process, although it is partly absorbed by the carbonates.[8,9] Lu *et al.*[10] decomposed biomass (boiled coffee beans) in molten carbonates at 800 °C and a molten chloride at 850 °C to obtain carbon with a specific morphology. In both cases, they obtained micrographite with a high specific area. Finally, more recently Zeng *et al.*[11] demonstrated the degradation of bio-oil to form syngas when treating biomass with molten carbonate pyrolysis at 850 °C.

In their search for solutions for the treatment of WEEE (Waste from Electrical and Electronic Equipment), mixed wastes containing different metals, plastics and resin/fibreglass composites, Flandinet *et al.*[12] suggested using molten hydroxides. Although not well studied so far, this family of molten salts offers interesting characteristics compared to molten carbonates, such as their lower melting temperature implying a lower energy cost, their high solubility of gases such as halogens[3] and CO_2 (which limits toxic emissions), and their high solubility of oxides, glasses and plastics.[13–15] In his study, Flandinet *et al.* demonstrated the benefits of molten hydroxides for the recovery of metals from WEEE also leading to production of H_2, which can potentially be recovered.

More recently Dai *et al.*[16] have focused on molten hydroxide media for the detoxification of chlorinated waste, with the aim

[a]*Unité de Catalyse et Chimie du Solide (UCCS), Université de Lille, 59655 Villeneuve d'Ascq, France. E-mail: sylvie.daviero@univ-lille.fr*

[b]*Laboratoire de Spectrochimie pour l'Interactions, la Réactivité et l'Environnement (LASIRE), Université de Lille, 59655 Villeneuve-d'Ascq, France*

[c]*Laboratoire Physico-Chimie des Electrolytes et Nanosystèmes Interfaciaux (PHENIX), CNRS, Sorbonne Université, 75005 Paris, France. E-mail: anne-laure.rollet@sorbonne-universite.fr*

† Electronic supplementary information (ESI) available. See DOI: https://doi.org/10.1039/d3ra02537c

to prevent dioxin production and to capture the chlorine produced during the degradation of the organic wastes. XRD and IR analysis of their residues after degradation shows a loss of organic hydrogen and chlorine after treatment, and the presence of KCl in the bath. This demonstrates the absorption of halogens in the hydroxide baths and their advantage of avoiding the release of acid gases and dioxins.

Their study also shows that gas scrubbing is directly related to the travel time in the molten salt bath and therefore the importance of the salt/waste volume ratio that must be sufficient to treat the emitted gases. Furthermore, they propose a reaction mechanism with alkaline hydroxides (MOH), similar to those in molten carbonates in the MSO process, leading to formation of alkaline chloride salt (MCl), water and carbon dioxide according to the equation:

$$C_6H_3Cl_3 + MOH + O_2(g) \rightarrow MCl + CO_2(g) + H_2O(g) + \text{intermediate products}$$

The objective of our study is to understand more deeply the mechanisms involved in the treatment of organic compounds and polymers in molten salt hydroxide baths. For this purpose, we have treated simple organic molecules ranging from short-chain carboxylic acids up to more complex chlorinated polymers. We have analyzed the solid and gaseous reaction products using complementary techniques. In contrast to what happens in molten carbonates, the hydroxide baths do not correspond to the standard reaction mechanisms described in MSO and we propose a new process adapted to the molten hydroxides.

2 Experimental setup and protocols

2.1 Setup description

A specific setup, described in Fig. 1, has been developed to carry out the experiments in molten hydroxide media. It is divided into three main parts: (i) the incoming gas to control the reactor atmosphere and in-bath bubbling (blue zone in Fig. 1); (ii) the main reaction apparatus is made of a heated stainless steel reactor where a protective graphite crucible contains the glassy carbon crucible where the molten salt bath will react (red zone); and (iii) the exhaust gas circuit (yellow zone) connected to a mass spectrometer (MS). The sample insertion is performed once the bath is molten and thermally stabilized *via* an opening hatch on the top of the reactor.

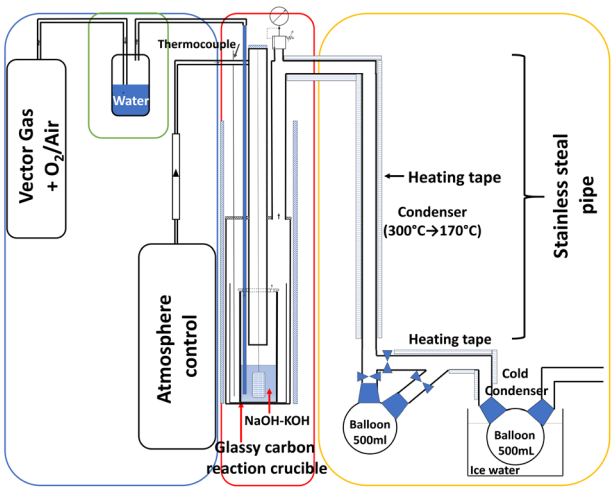

Fig. 1 Scheme of the setup: the blue zone shows the gas control, the red zone shows the main reaction apparatus with an inox 316L reactor and glassy carbon crucible containing the salt and gold cage, and the yellow zone shows the exhaust gas circuit.

2.2 General reaction protocol

100 g of salt mixture (75% mol NaOH/25% mol KOH, $T_{melting}$ = 250 °C) are introduced into the glassy carbon crucible and heated at 400 °C. The controlled atmosphere on the bath surface is argon (flow rate 30 L h^{-1}) and the bubbling gas is a mixture of 80% Ar and 20% O_2, humidified by passing through water heated at 80 °C, allowing control of the humidity and acidity of the bath. The experiment starts when the sample is introduced in the molten salt through the hatch at the top of the reactor. In order to obtain a perfect immersion of the sample in the molten salt and avoid its reaction on the surface of the bath (*i.e.* a simple thermal degradation due to heat without interaction with the bath), it is placed into a gold cage (1.5 cm high, 1 cm wide and 1 cm thick), see ESI (Fig. S1†). The same sample mass is used for both organic acids and polymers, *i.e.* approximately 1 g. The carboxylic acids are frozen in liquid nitrogen before being placed into the gold cage for a rapid immersion into the molten salt. Butanoic acid (4 C), hexanoic acid (6 C) and decanoic acid (10 C) are successively introduced into the same bath. After each reaction, the gold cage is removed using an attached gold wire. It is then cleaned and filled with the subsequent carboxylic acid. After 5 hours of reaction, the furnace is switched off and left to cool down to room temperature. The solidified bath is then recovered; a part is collected for bath analysis after the reaction, the other part is dissolved in 500 ml of distilled water and filtrated to recover the solid residues for analysis. The three different kinds of sample (carboxylic acids, neoprene and polyethylene) are treated in three different baths. For specific experiments on exhaust gas and electrochemical *in situ* analysis, the bubbling gas is dried to avoid saturation of the mass spectrometer with water and to allow the evolution of the water content in the bath to be monitored electrochemically.

2.3 Analysis

2.3.1 X-ray diffraction. Powder X-ray diffraction was performed on a Bruker D8 Advance diffractometer (Bragg–Brentano geometry, using monochromated Cu K-α radiation and a Ni filter, with 0.02° 2θ steps and 0.5 seconds per step) and the resulting patterns checked with the DIFFRAC.EVA software (Brucker AXS). Due to being highly hygroscopic, the bath samples were prepared in a glove box under an argon atmosphere and protected from atmospheric humidity by a Mylar film.

2.3.2 Infrared and Micro-Raman spectroscopies. Infrared analysis (IRTF) was performed using a PerkinElmer Spectrum

Two spectrometer over the 4000–400 cm^{-1} spectral range with 10 accumulations and 4 cm^{-1} step. Micro-Raman analyses were performed with a LabRAM HR Evolution (HORIBA Scientific) microspectrometer using a 50X 0.9 NA Olympus objective. The spectrometer is equipped with a 600 lines per mm grating and excitation was carried out using 515 nm radiation.

2.3.3 Electron paramagnetic resonance (EPR) spectroscopy. Pulsed EPR experiments at X-band were performed using a Bruker ELEXSYS E-580 spectrometer with a SuperX-FT microwave bridge and a Bruker ER EN4118X-MD4 dielectric resonator. Cryogenic temperatures (10 K and 50 K) were obtained using an Oxford flow cryostat. The field-swept EPR spectra were recorded by electron spin echo (ESE) detection; electron spin echo (ESE)-detected EPR experiments were carried out with the pulse sequence of $\pi/2$–τ–π–τ–echo. The microwave (mw) pulse lengths $t_{\pi/2} = 16$ ns and $t_{\pi} = 32$ ns and a τ value of 204 ns were used. A two-step phase-cycle was applied to remove all unwanted echoes. The Hyperfine Sublevel Correlation (HYSCORE) experiments were carried out using the pulse sequence $\pi/2$–τ–$\pi/2$–t_1–π–t_2–$\pi/2$–τ–echo, with $t_{\pi/2} = 16$ ns and $t_{\pi} = 32$ ns and a τ value of 132 ns for the X-band. Different τ values have also been checked to identify blind spots affecting the 2D HYSCORE experiments. The time traces of the HYSCORE spectra were baseline-corrected using a third-order polynomial, apodized with a Hamming window and zero-filled. After two-dimensional Fourier transformation, the absolute value spectra were calculated. A four-step phase cycle has been used to remove unwanted echoes.

2.3.4 Electrochemical measurements. The electrochemical tests were conducted in a three-electrode electrochemical cell using a potentiostat/galvanostat Biologic BP-300 controlled by EC-Lab. Pt wire (99.9% purity, 0.5 mm diameter) was used as a working electrode; it was submerged 2.3 cm in the bath. A home-made Ag/AgCl (2×10^{-2} M NaCl in $LiNO_3$–$NaNO_3$) was used as a reference electrode. It consisted of an Ag wire (99.9% purity, 1 mm diameter) coated with AgCl, which is immersed in 46.3% mol $LiNO_3$–53.7% mol $NaNO_3$ eutectic salt containing 2×10^{-2} M NaCl and using an alumina tube as the compartment. A graphite rod (4.8 mm diameter) was used as a counter electrode. Pt and Ag wires were obtained from Goodfellow, while the alumina tube and graphite rod were obtained from Final Advanced Materials.

Linear sweep voltammetry (LSV) was used to follow the evolution of the acidity of the NaOH–KOH bath before and after the reaction. The bath was dried for 72 h at 400 °C under an atmosphere of dry Ar prior to adding the polymer.

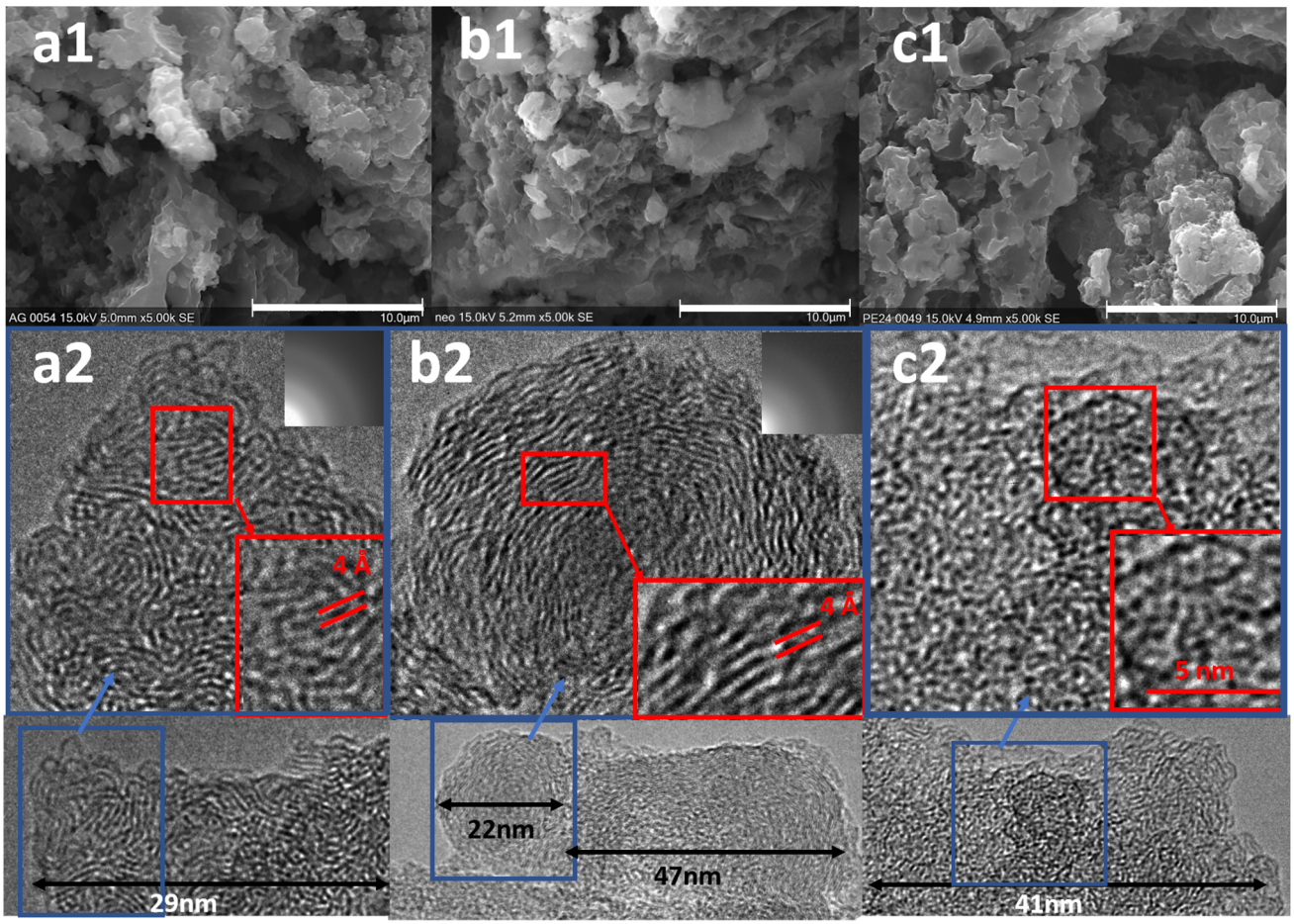

Fig. 2 SEM (1) and TEM/HRTEM images with various enlargements and corresponding diffraction patterns (2) of solid residues after treatment: (a) carboxylic acid residue, (b) neoprene residue, and (c) polyethylene residue. The distances between distorted graphite sheets are indicated.

2.3.5 SEM and TEM. SEM images were taken on a scanning electron microscope, FlexSem1000 with an accelerating voltage of 15 kV at 5k magnification. High-resolution images of ground and dispersed samples on a carbon membrane grid were obtained on a FEI Tecnai G2-20 TWIN transmission microscope.

2.3.6 Mass spectroscopy. The gases released during the reaction were analysed with a Transpector® MPS100 Inficon mass spectrometer, *m*/*z* 0–100, FabGuard Explorer software, which can identify the gases released but not quantify them directly, such that only the relative ratios can be determined.

3 Results and discussion

3.1 Solid residue analysis

To give insight into the mechanisms of the organic solids decomposition reaction in the hydroxide baths, different kinds of organic compounds were used. First, two polymers were selected: polyethylene that contains only C–H chains and neoprene that also contains chlorine. Second, a series of short linear-chain organic acids was used (butanoic acid 4 C, hexanoic 6 C and decanoic 10 C) in order to determine if the decomposition products are similar between these two families of organic solids.

SEM and TEM images of the solid residues obtained after treatment of (a) carboxylic acids, (b) neoprene, and (c) polyethylene are shown in Fig. 2. As the three carboxylic acids were treated consecutively in the same experiment, the sample contains a mixture of the three residues. In all cases, sheets of similar size and shape are observed (Fig. 2(a1)–(c1)). Furthermore, they resemble those observed by Lu *et al.*[10] for boiled coffee beans treated in molten Na_2CO_3–K_2CO_3 at 800 °C, as well as by Gu *et al.*[17] in the treatment of semi-coke at 500–700 °C in $ZnCl_2$–KCl. The resulting sheets were identified as carbon graphite particles. As shown in the TEM images in Fig. 2(a2) and (b2) of carboxylic acid and neoprene residues, respectively, organised crystal planes are clearly observable in nanodomains indicating the area of the crystallised graphite sheets. The distance between the sheets is around 4 Å larger than what is expected in well-crystallized graphite (3.3–3.5 Å (ref. 18 and 19)). According to the literature, this difference can be explained by significant disruption to the ordered graphite structure, leading to warping, delamination, dislocations, and defects, as described in the article of Welham *et al.*[20] In the polyethylene residue Fig. 2(c2), a disorder is observed with some areas of organised planes at the edge, indicating a more amorphous sample than the others.

To investigate further, IR analysis has been performed on the solid residues. Very similar spectra for carboxylic acids and neoprene are obtained after the reactions (Fig. 3b and d). None of the characteristic bands of the carboxylic acids (broad O–H stretching band at 3300–2500 cm^{-1}, C=O stretching at 1700 cm^{-1}, or O–H bending at 1430 cm^{-1}) can be observed, nor the C–Cl stretching bands (800 cm^{-1}) for the neoprene residue. In all cases, the characteristic C–H bands have disappeared and only vibrations associated with carbon bonds (stretching modes for C=C at 1645 cm^{-1} and for C–C at 1200 and 1375 cm^{-1}) can be slightly observed. Furthermore, the spectrum is similar to that of graphite residues obtained after the calcination of coconut shells at 1023 K.[21]

For polyethylene (Fig. 3f), the C–H stretching and bending bands are strongly attenuated after treatment, revealing a profile very close to the neoprene spectrum after the reaction.

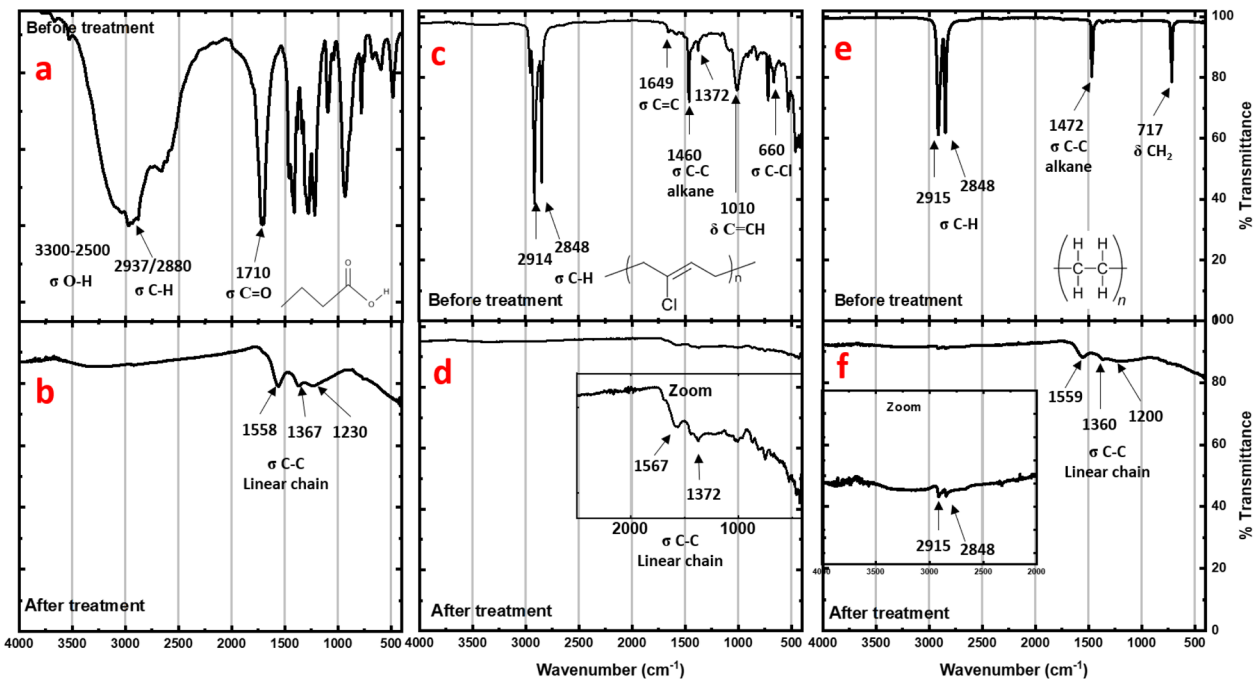

Fig. 3 IR spectra of residues before (top) and after (bottom) treatment of carboxylic acids (a and b), neoprene (c and d), and polyethylene (e and f).

However, even with weak intensity, the presence of these residual C–H stretching and bending bands observed after treatment indicates incomplete degradation. This explains the higher disorder observed using TEM on the corresponding residue sheets.

To better characterize the graphite particles, Raman analysis was carried out on the residue of neoprene after the reaction. The bands observed in the spectra are deconvoluted following the Kawakami method[22] allowing us to attribute the different bands observed to different hybridizations of the carbons. The G band (corresponding to graphite) observed around 1580 cm^{-1} is attributed to the sp^2 carbon bonded to the other carbons. The others bands appearing around 1360 cm^{-1} and 1680 cm^{-1}, known as the D and D′ bands, respectively, correspond to a "defect structure" attributed to sp^2 hybridized carbon at the edges of the graphite sheets. All the discussions below will use this nomenclature. The deconvolution of the Raman spectrum (Fig. 4) shows the presence of G, D and D′ bands at 1586, 1357 and 1693 cm^{-1} respectively. In addition, three bands corresponding to random contributions (R) according to Kawakami nomenclature were also extracted.[22] These R bands would correspond to a random structure that is intermediate between graphite and an amorphous structure. The spectrum shape is much like the one of graphite produced by heat treatment (773 K) under CO_2 of bamboo charcoal.[22] It is worth noting that, in agreement with the IR results, no C–H bands were observed.

Moreover, part of the solidified salt was analyzed by X-ray diffraction after each treatment to check the salt stability. No carbonate phase was observed (Fig. 5), thus confirming the absence of CO_2 dissolved in the bath. The large non-indexed peak at 26° corresponds to the polyethylene terephthalate (Mylar®) used as moisture protection of the XRD samples. Finally, the salts that mark the chloride absorption by the bath (KCl and NaCl) were not observed, probably due to the too small quantities formed. In our experimental conditions 1 g of treated neoprene contains approximately 0.34 g of chlorine which will be disolved in 100 g of bath, this ratio is below the limits of phases detection by powder XRD.

The diffraction pattern of the carboxylic acid residue presented in Fig. 6 shows two broad and weak peaks indicating low crystallinity or the presence of nanoparticles. This diffraction pattern is similar to the residue obtained by Lu *et al.*[10] The peak located around 22° corresponds to the (002) reflection of a graphitic network and the one at 43° corresponds to a disordered stacking of the micrographite sheets.

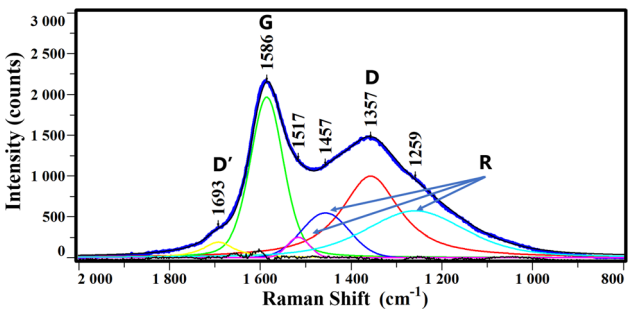

Fig. 4 Raman spectrum of neoprene residue after treatment (thick blue line) and the deconvolution into D′ (yellow), G (green), R (magenta, blue, cyan) and D (red) bands.

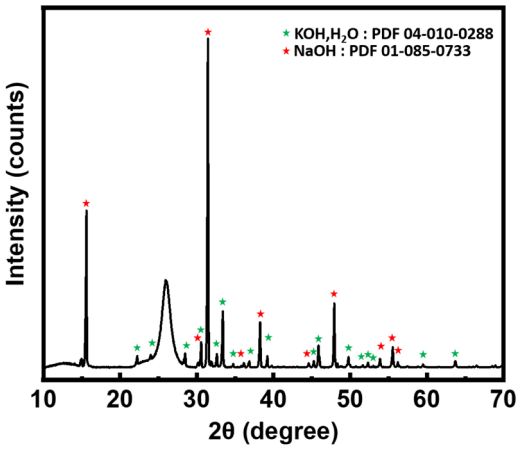

Fig. 5 X-ray diffraction pattern of salt after treatment. KOH peaks denoted by green stars and NaOH peaks denoted by red stars.

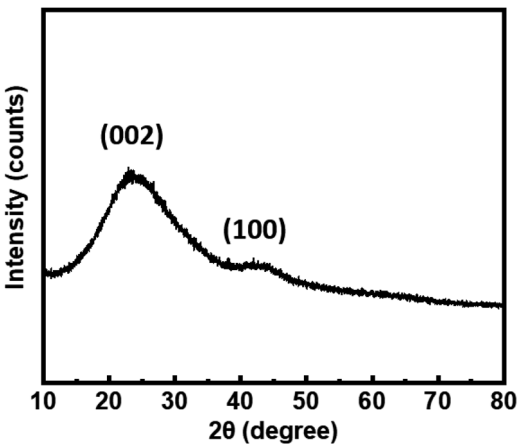

Fig. 6 Powder X-ray diffraction pattern of carboxylic acid residue after treatment in molten hydroxide. The indexed peaks correspond to characteristic peaks of low-crystallinity graphite.

In all cases, without considering the size of the initial organic chain, the degradation in molten hydroxides yields the formation of solid carbon residues. The composition of the latter is close to that of graphite obtained after the calcination of organic fibers like bamboo or coconuts shells.

Finally, complete mass balance cannot be performed due to observed losses during the recovery of the solid graphite fraction on the filter and in the filtrate, as detailed in the ESI.† However, an estimation is provided by comparing the experimental results of the CHONS elemental analysis (ESI†) of neoprene with the mass of residue obtained.

3.2 Gas and fumes analysis

During the degradation experiment, the gas and fumes were analysed for each sample using mass spectrometry (Fig. 7a, 8 and 9, and Fig. S2 and S3 in the ESI†). It should be remembered

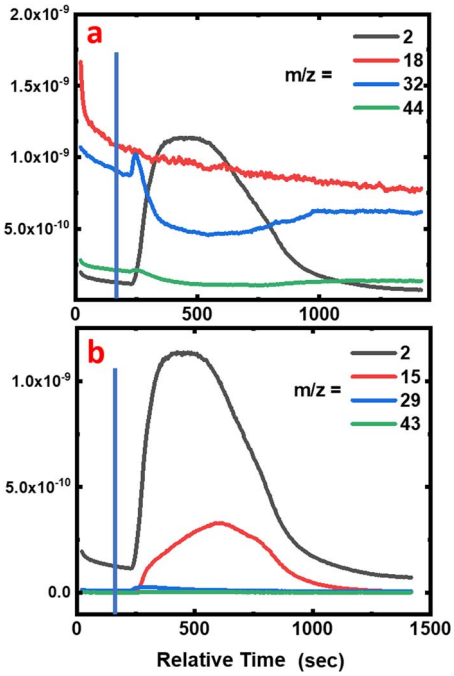

Fig. 7 Mass spectra of gas emitted during the treatment of butanoic acid. The vertical line corresponds to the insertion of sample after a stabilization time of the atmosphere. Spectrum (a) with $m/z = 2$ for H_2, 18 for H_2O, 32 for O_2 and 44 for CO_2, and spectrum (b) relative comparison in alkanes/H_2 intensity with $m/z = 2$ for H_2, 15 for CH_3, 29 for C_2H_5 and 43 for C_3H_7.

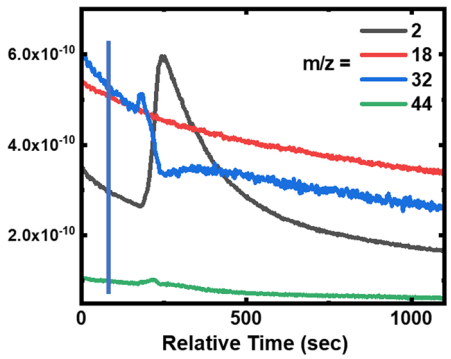

Fig. 8 Mass spectra of gas during treatment of neoprene with $m/z = 2$ for H_2, 18 for H_2O, 32 for O_2 and 44 for CO_2. The vertical line corresponds to the insertion of sample after a stabilization time of the atmosphere.

that in this particular case, reactions are carried out in a dry atmosphere to avoid saturating the mass spectrometer with water. The striking points are the production of dihydrogen ($m/z = 2$), along with the decrease of O_2 concentration ($m/z = 32$), but without any CO_2 and gaseous H_2O production ($m/z = 44$ and 18, respectively). Flandinet *et al.*[12] had already observed the release of H_2 during printed circuit board degradation and already proposed a possible recovery.

No other species were observed after the polymers' treatment. In the specific case of the neoprene, the chlorine present

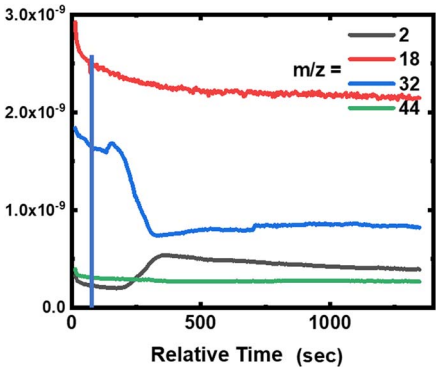

Fig. 9 Mass spectra of gas during treatment of polyethylene with $m/z = 2$ for H_2, 18 for H_2O, 32 for O_2 and 44 for CO_2. The vertical line corresponds to the insertion of sample after a stabilization time of the atmosphere.

in the polymer is not visible in the gases emitted, which is in agreement with the study by C. Lin *et al.*[7] that shows that chlorides produced during the reaction in molten salts are absorbed up to 99.99%. On the contrary, for carboxylic acids, the mass spectra reveal the presence of light alkanes in addition to dihydrogen (Fig. 7b and in the ESI, Fig. S2 and S3†). Due to their low vaporization temperature, a small fraction of acid is likely to be evaporated when introduced into the reaction chamber. In consequence, this small amount of acid undergoes partial thermal degradation in the reactor atmosphere, leading to the formation of these alkanes. This hypothesis is corroborated by the fact that the highest content of alkanes is observed for the degradation of butanoic acid, whose vaporization temperature is the lowest (Fig. 7b compared with the figures for hexanoic and decanoic acids given in the ESI, Fig. S2 and S3,† respectively). In addition, one must note from the mass spectra that the end of the reaction corresponds to the decrease of the H_2 production associated with an increase of O_2 in the atmosphere.

Furthermore, the absence of CO_2 production during the reaction can be related to the solid graphite residue formation in the bath. Concerning the absence of H_2O in the emitted gas, this points to possible water formation linked with the diminution of O_2 content in the atmosphere during the reaction, and its dissolution in the dry hydroxide bath.

To confirm this hypothesis, *in situ* electrochemical analyses have been performed in the molten bath during a treatment of neoprene. The LSV voltammograms (Fig. 10) show a peak at −1.8 V corresponding to the reduction of H_2O to H_2. A significant increase in current, from −40 mA cm^{-2} to −450 mA cm^{-2}, is observed after adding neoprene. This supports the theory of released water being dissolved in the bath and generating an increment of Lux-Flood acidity.[23,24]

3.3 Proposed reaction mechanisms in molten hydroxides

3.3.1 Solubilization of oxygen. According to the literature, molten salts, as well as aqueous media, can solubilise gases, especially oxygen. For instance, it was evidenced by Volkovich

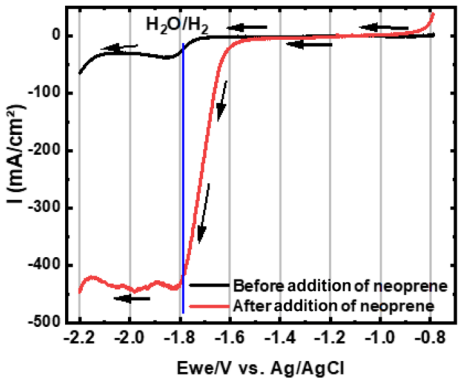

Fig. 10 Linear sweep voltammograms at 500 mV s^{-1} of molten hydroxide, before (black line) and after (red line) addition of neoprene. The blue line corresponds to the potential reduction of the water in the bath.

et al.[25] and by Hayashi *et al.*[24] in molten carbonate and molten hydroxide, respectively. The oxygen is solubilized into its peroxide ion form according to the following equation:

$$\tfrac{1}{2}O_2 + 2OH^- \rightarrow {O_2}^{2-} + H_2O$$

As a reminder, in molten hydroxide there are different species of oxygen ions (oxide, peroxide and superoxide) based on the following redox equations:[23]

$${O_2}^{2-(-I)} + 2e^- \rightleftharpoons 2O^{2-(-II)}$$

and

$${O_2}^{-(-0,5)} + e^- \rightleftharpoons {O_2}^{2-(-I)}$$

The increase in the oxygen potential relative to oxygen activity, pO^{2-}, leads to dismutation of peroxide ions:

$$3{O_2}^{2-(-I)} + 2H_2O^{(-II)} \rightarrow 2{O_2}^{-(-0,5)} + 4OH^{-(-II)}$$

and considering the hydroxide autoprotolysis:

$$2OH^- \rightleftharpoons H_2O + O^{2-}$$

The equilibrium of oxygen ions can be simplified by:

$$3{O_2}^{2-(-I)} \rightleftharpoons 2{O_2}^{-(-0,5)} + 2O^{2-(-II)}$$

This shows that ion oxide is formed by the dissolution of oxygen (O_2) to peroxide (O_2^{2-}) and the dismutation of peroxide to oxide and superoxide (O_2^-).

3.3.2 Consumption of oxygen and formation of hydroxyl radicals. Following Takanabe *et al.*[26] and Yao *et al.*,[27] the formation of hydroxyl radicals can be explained by the presence of oxidising species that react to form hydroxyl radicals *via* two possible reactions:

$$O_2 + H_2O \rightarrow 4OH^\bullet$$

or

$${O_2}^{2-} + H_2O \rightarrow O^{2-} + H_2O_2$$

and

$$H_2O_2 \rightarrow 2OH^\bullet$$

Simplified by (with H_2O_2 intermediate species):

$${O_2}^{2-} + H_2O \rightarrow 2OH^\bullet + O^{2-} \quad (1)$$

There are therefore various oxidising and radical species present in the hydroxide bath that can lead to various reactions (redox, acid–base and radical) depending on the material in the bath.[23]

3.3.3 Degradation mechanism. Dai *et al.* have demonstrated in their study on the degradation of chlorine-containing waste in molten NaO–KOH that chlorine is retained in the salt in chloride ion form and that there is a low impact on the composition of the molten salt, with no carbonate being detected,[16] from Energy Dispersive X-ray (EDX) quantification. They have determined 36% loss of carbon and deduced that an equivalent production of CO_2 may have occurred. Based on these observations, they suggested an oxidation mechanism in the molten hydroxides, similar to MSO in molten carbonates,[8] where the gases emitted are essentially H_2O and CO_2. However, in our working conditions, the analysis of the gas and fumes with mass spectrometry reveals no H_2O or CO_2 gas production during the reaction and the organic matter degradation at 400 °C leads to solid graphite and H_2 gas production. This raises the question about the mechanisms involved and that these seem not to be similar to MSO-type ones in this case, despite the potential presence of different oxidizing species. Therefore, a different route was considered.

The reaction products obtained here are similar to a non-oxidative cracking reaction as occurs in petrochemistry,[28] where the mechanisms involved are radical in nature. The presence of hydroxyl radicals $OH^\bullet$ in molten hydroxides makes such a mechanism possible.[26,27] In accordance with the various analyses carried out during the experiments, as well as the end products obtained, an analogous mechanism can be proposed for the organic molecule degradation leading to H_2 and carbon graphite formation:

$$C_xH_y + OH^\bullet \rightleftharpoons C_xH_{y-1}^\bullet + H_2O \quad (2)$$

$$C_xH_{y-1}^\bullet \rightleftharpoons C_xH_{y-2} + H^\bullet$$

until

$$C_xH_{y-(y+1)}^\bullet \rightleftharpoons C_x + H^\bullet \quad (3)$$

$$H^\bullet + H^\bullet \rightarrow H_2 \quad (4)$$

The consumption of oxygen can be explained by the formation of oxygen ion compounds in molten hydroxide; the reaction of oxygen and the peroxide ion with water forms hydroxyl radicals, as seen in eqn (1). Graphite is formed during the release of radical hydrogens from the carbon chains, as shown in eqn (3). Moreover, the chain radicals involved in eqn (2) allow longer chain recombination, as shown by Choudhary *et al.*[28] following eqn (5).

$$2C_xH_{y-1}^{\cdot} \rightleftharpoons C_{2x}H_{2y-2} \quad (5)$$

Hence, graphite sheets can be formed, composed of many more carbons than the organic species they are derived from. The graphite, identified in the SEM image after the carboxylic acid degradation typifies this phenomenon.

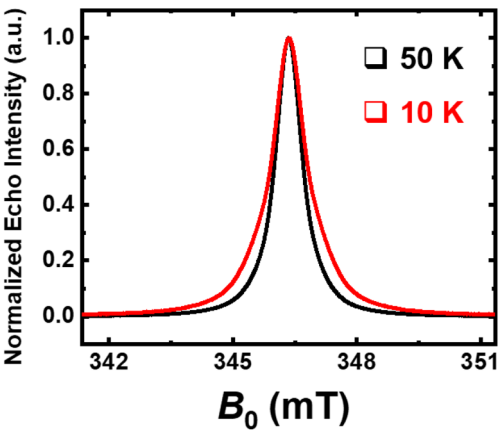

Fig. 11 Echo-detected field-swept (ED-FS) spectra recorded at an X-band frequency (9.7 GHz) on neoprene residue after treatment; $T = 50$ K (black line) and $T = 10$ K (red line).

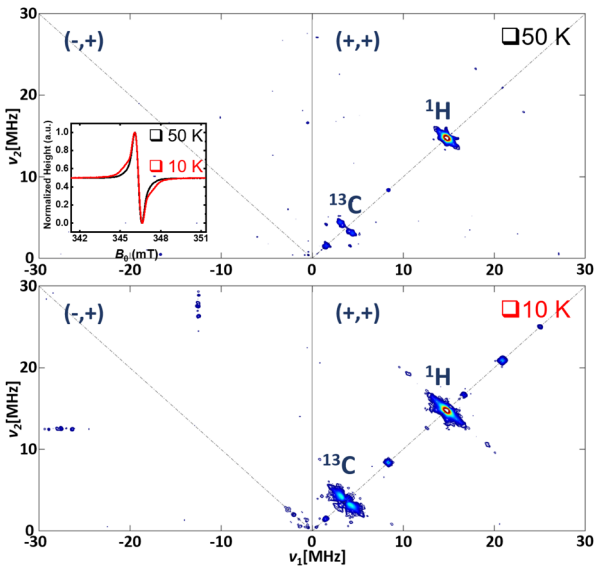

Fig. 12 HYSCORE spectra recorded at an X-band frequency (9.7 GHz); $T = 50$ K (top) and $T = 10$ K (bottom). Inset: pseudo-modulation of the ED-FS as for Fig. 11.

To corroborate this mechanism, the identification of radicals species has been done using Electron Magnetic Resonance (EMR) analysis, and has thus been performed on a neoprene residue after treatment (Fig. 11). A very intense and extremely narrow line that can be well simulated with a single Lorentzian component is observed. The measured g-factor of 2.0036(4) is very close to the electron free value and indicates it is due to the carbon-based states, thus confirming the existence of carbon radicals in the sample. The half-width full-maximum $\Delta H_{\frac{1}{2}}$ of this resonance is only 0.74 mT, in agreement with reported graphite-like samples.[29] At 10 K, further broadening is observed, suggesting the presence of more than one carbon-based species, *i.e.*, at least two carbon radicals with different environments.

In order to identify the nuclei coupled to the radical species, Hyperfine Sublevel Correlation (HYSCORE) spectroscopy has been used (Fig. 12).[30] Indeed, ^{1}H and ^{13}C nuclear Larmor frequencies can be observed on the HYSCORE spectrum, both at 50 K and 10 K, on the (+,+) quadrant, for weakly coupled nuclei.

4 Conclusions

This study showed the degradation at 400 °C of low molar mass organics, carboxylic acids, and complex polymers in molten hydroxides. We were able to analyse and characterise the different reaction products (solid and gaseous) obtained during the degradation. These products, essentially graphite and dihydrogen, are the same for the reactions involving carboxylic acids, polyethylene and neoprene. The formation of graphite without the production of CO_2 indicates that the reaction cannot correspond to an oxidation reaction as usually described in MSO processes. The analysis of the solid residues and previous studies show the presence of radical species in the molten hydroxide salts. We therefore propose a radical mechanism associated with this treatment to explain more accurately the reactions involved in molten hydroxide salts. It is important to work on the optimisation of the process, in particular the working temperature and the oxygen injection rate, as well as the salt/waste mass ratio depending on the nature of the waste. Overall this process, which makes it possible to treat microplastics, is a promising sustainable method for hydrogen and graphite recovery without greenhouse gas emissions.

Author contributions

Conceptualization: F. Lecomte, A.-L. Rollet, S. Daviero-Minaud. Formal analysis: F. Lecomte, A. Moissette, A.-G. Porras-Guitérrez, G. Sicoli, M. Huve. Funding acquisition: A.-G. Porras-Guitérrez, A.-L. Rollet, S. Daviero-Minaud. Investigation: F. Lecomte, A.-G. Porras-Guitérrez, G. Sicoli, M. Huve. Methodology: F. Lecomte, A.-L. Rollet, S. Daviero-Minaud. Project administration: F. Lecomte, A.-L. Rollet, S. Daviero-Minaud. Supervision: A.-L. Rollet, S. Daviero-Minaud. Writing – original draft: F. Lecomte, S. Daviero-Minaud. Writing – review & editing: F. Lecomte, A.-L. Rollet, S. Daviero-Minaud, A. Moissette, A.-G. Porras-Guitérrez.

Conflicts of interest

There are no conflicts to declare.

Acknowledgements

This study was made possible by the CNRS in the context of F. Lecomte's PhD thesis. The authors also thank the Chevreul Institute for XRD and microscopy platforms, LASIRE for the Raman spectroscopy experiments and EPR, PHENIX for the electrochemistry experiments, and UCCS for providing the various analysis platforms and laboratories.

Notes and references

1 Association of Plastic Manufacturers, Plastics – the Facts 2020, *PlasticEurope*, 2020, p. 16.
2 P. Kovařík, J. D. Navratil and J. John, Scientific and engineering literature mini review of molten salt oxidation for radioactive waste treatment and organic compound gasification as well as spent salt treatment, *Sci. Technol. Nucl. Install.*, 2015, **2015**, 407842.
3 H.-C. Yang, Y.-J. Cho, J.-S. Yun and J.-H. Kim, Destruction of Halogenated Plastics in a Molten Salt Oxidation Reactor, *Can. J. Chem. Eng.*, 2003, **81**, 713–718.
4 A. Fedorov, Y. Chekryshkin and A. Gorbunov, Studies of Recycling of Poly(vinyl chloride) in Molten Na, Ca||NO_3, OH Systems, *ISRN Chem. Eng.*, 2012, 768134.
5 H. C. Yang, Y. J. Cho, H. C. Eun and E. H. Kim, Destruction of chlorinated organic solvents in a two-stage molten salt oxidation reactor system, *Chem. Eng. Sci.*, 2007, **62**, 5137–5143.
6 Z. Ismagilov, M. Kerzhentsev and M. Adamson, *Scientific Advances in Alternative Demilitarization Technologies*, 2015, vol. 6, pp. 29–48.
7 C. Lin, Y. Chi, Y. Jin, X. Jiang, A. Buekens, Q. Zhang and J. Chen, Molten salt oxidation of organic hazardous waste with high salt content, *Waste Manage. Res.*, 2018, **36**, 140–148.
8 M. G. Adamson, P. C. Hsu, D. L. Hippie, K. G. Foster, R. W. Hopper and T. D. Ford, Organic waste processing using molten salt oxidation, *High Temp. Mater. Process.*, 1998, **2**, 559–580.
9 P. C. Hsu, K. G. Foster, T. D. Ford, P. H. Wallman, B. E. Watkins, C. O. Pruneda and M. G. Adamson, Treatment of solid wastes with molten salt oxidation, *Waste Manage.*, 2000, **20**, 363–368.
10 B. Lu, J. Zhou, Y. Song, H. Wang, W. Xiao and D. Wang, Molten-salt treatment of waste biomass for preparation of carbon with enhanced capacitive properties and electrocatalytic activity towards oxygen reduction, *Faraday Discuss.*, 2016, **190**, 147–159.
11 K. Zeng, J. Li, Y. Xie, H. Yang, X. Yang, D. Zhong, W. Zhen, G. Flamant and H. Chen, Molten salt pyrolysis of biomass: The mechanism of volatile reforming and pyrolysis, *Energy*, 2020, **213**, 118801.
12 L. Flandinet, F. Tedjar, V. Ghetta and J. Fouletier, Metals recovering from waste printed circuit boards (WPCBs) using molten salts, *J. Hazard. Mater.*, 2012, **213–214**, 485–490.
13 B. Trémillon, *Chemistry in Non-Aqueous Solvents*, 1967.
14 L. Chen, J. Yang, Y. Yang, J. Yu, X. Hu, W. Tao and Z. Wang, Solubility and dissolution behavior of ZrO_2 in KF–AlF_3 molten salts, *J. Mol. Liq.*, 2022, **347**, 118037.
15 L. C. Yu, C. Clark, X. Liu, A. Ronne, B. Layne, P. Halstenberg, F. Camino, D. Nykypanchuk, H. Zhong, M. Ge, W. K. Lee, S. Ghose, S. Dai, X. Xiao, J. F. Wishart and Y. C. K. Chen-Wiegart, Evolution of micro-pores in Ni-Cr alloys *via* molten salt dealloying, *Sci. Rep.*, 2022, **12**, 20785.
16 S. Dai, Y. Zheng, Y. Zhao, Y. Chen and D. Niu, Molten hydroxide for detoxification of chlorine-containing waste: Unraveling chlorine retention efficiency and chlorine salt enrichment, *J. Environ. Sci.*, 2019, **82**, 192–202.
17 Y. Gu, Y. Tang, L. Liu, Y. Zhang, Y. Gao, Y. Zhang, C. Yang and T. Liu, Semi-coke-based amorphous porous carbon synthesized by a molten salt assisted method for superior lithium storage, *New J. Chem.*, 2023, **47**, 2907–2913.
18 J. Li, Y. Qin, Y. Chen, Y. Song and Z. Wang, HRTEM observation of morphological and structural evolution of aromatic fringes during the transition from coal to graphite, *Carbon*, 2022, **187**, 133–144.
19 A. R. Kamali and J. Yang, Effect of molten salts on the structure, morphology and electrical conductivity of PET-derived carbon nanostructures, *Polym. Degrad. Stab.*, 2020, **177**, 109184.
20 N. J. Welham, V. Berbenni and P. G. Chapman, Effect of extended ball milling on graphite, *J. Alloys Compd.*, 2003, **349**, 255–263.
21 M. J. Rampe, B. Setiaji, W. Trisunaryanti and T. Triyono, Fabrication and Characterization of Carbon Composite From Coconut Shell Carbon, *Indones. J. Chem.*, 2011, **11**, 124–130.
22 M. Kawakami, T. Karato, T. Takenaka and S. Yokoyama, Structure analysis of coke, wood charcoal and bamboo charcoal by Raman spectroscopy and their reaction rate with CO_2, *ISIJ Int.*, 2005, **45**, 1027–1034.
23 B. Trémillon, Diagrammes d'équilibre potentiel-acidité (E-p02-) dans les sels et hydroxydes alcalins fondus, *Pure Appl. Chem.*, 1971, **25**, 395–428.
24 H. Hayashi, S. Yoshizawa and Y. Ito, Studies on oxygen reduction in molten NaOH, *Electrochim. Acta*, 1983, **28**, 149–153.
25 V. A. Volkovich, T. R. Griffiths, D. J. Fray and M. Fields, Increased oxidation of UO_2 in molten alkali-metal carbonate based mixtures by increasing oxygen solubility and by controlled generation of superoxide ions, and evidence for a new sodium uranate, *J. Chem. Soc., Faraday Trans.*, 1997, **93**, 3819–3826.
26 K. Takanabe, A. M. Khan, Y. Tang, L. Nguyen, A. Ziani, B. W. Jacobs, A. M. Elbaz, S. M. Sarathy and F. F. Tao, Integrated *In Situ* Characterization of a Molten Salt Catalyst Surface: Evidence of Sodium Peroxide and

Hydroxyl Radical Formation, *Angew. Chem., Int. Ed.*, 2017, **56**, 10403–10407.

27 Z. Yao, X. Zhao and J. Li, Study on 1,2,3-Trichlorobenzene Destruction in a Binary $(Na,K)_2CO_3$ Molten Salt Oxidation System, *Environ. Prog. Sustainable Energy*, 2014, **33**, 65–69.

28 T. V. Choudhary, E. Aksoylu and D. W. Goodman, Nonoxidative activation of methane, *Catal. Rev.: Sci. Eng.*, 2003, **45**, 151–203.

29 C. I. Smith, H. Miyaoka, T. Ichikawa, M. O. Jones, J. Harmer, W. Ishida, P. P. Edwards, Y. Kojima and H. Fuji, Electron spin resonance investigation of hydrogen absorption in ball-milled graphite, *J. Phys. Chem. C*, 2009, **113**, 5409–5416.

30 J. Kausteklis, P. Cevc, D. Arčon, L. Nasi, D. Pontiroli, M. Mazzani and M. Riccò, Electron paramagnetic resonance study of nanostructured graphite, *Phys. Rev. B: Condens. Matter Mater. Phys.*, 2011, **84**, 125406.